PLAXIS

essential for geotechnical professionals

PLAXIS

The Frozen and Unfrozen Soil Model

2016

Edited by:

S.A. Ghoreishian Amiri
Norwegian University of Science and Technology, Norway

G. Grimstad
Norwegian University of Science and Technology, Norway

M. Aukenthaler
PLAXIS bv, The Netherlands

S. Panagoulias
PLAXIS bv, The Netherlands

R.B.J. Brinkgreve
Delft University of Technology & PLAXIS bv, The Netherlands

A. Haxaire
PLAXIS bv, The Netherlands

TABLE OF CONTENTS

SYMBOLS

LOWER CASE SYMBOLS

a_i	Coefficients for melting-pressure equation [-]
b_i	Exponents for the melting-pressure equation [-]
c_s	Specific heat capacity [J/(kg K)]
d_g	Geometric mean of the soil particle diameter [mm]
d_i	Arithmetic mean diameter of textural class *i* [mm]
e	Void ratio [-]
e_0	Initial void ratio [-]
k	Hydraulic conductivity [m/s]
k_{sat}	Saturated hydraulic conductivity [m/s]
k_t	Rate of change in apparent cohesion with suction [-]
m	Yield parameter [-]
m_i	Mass fraction of textural class *i* [%]
n	Porosity [-]
p^*	Effective mean stress [N/m^2]
p_{at}	Atmospheric pressure [N/m^2]
p_c^*	Reference stress [N/m^2]
p_f^*	Effective mean stress at the critical state of a frozen soil [N/m^2]
p_{ice}	Ice pressure [N/m^2]
p_{melt}	Melting pressure [N/m^2]
p_{ref}	Parameter for the pressure dependency of ice thawing temperature [N/m^2]
p_t	Vapour-liquid-solid triple point pressure [N/m^2]
p_w	Pore water pressure [N/m^2]
p_y^*	Pseudo pre-consolidation stress for a frozen condition [N/m^2]
$(p_{y0}^*)_{in}$	Initial pre-consolidation stress for unfrozen condition [N/m^2]
p_{y0}^*	Pre-consolidation stress for unfrozen condition [N/m^2]
Δp_{y0}^*	Rate of change in p_{y0}^* with depth [N/m^2]
q^*	Deviatoric stress [N/m^2]
q_f^*	Deviatoric stress at the critical state of a frozen soil [N/m^2]
r	Coefficient related to the maximum soil stiffness [-]
s_c	Cryogenic suction [N/m^2]
$s_{c,seg}$	Segregation threshold [N/m^2]
$(s_{c,seg})_{in}$	Initial segregation threshold [N/m^2]
t	Time [s]
w	Water content [m^3/m^3]
w_u	Unfrozen water content [m^3/m^3]

UPPER CASE SYMBOLS

E_f	Frozen Soil Young's Modulus [N/m^2]
$E_{f,ref}$	Frozen Soil Young's Modulus at a reference temperature [N/m^2]

$E_{f,inc}$	Rate of change in Young's modulus with temperature [N/(m^2 K)]
F_1	Yield criterion due to variation of solid phase [-]
F_2	Yield criterion due to variation of suction [-]
G	Soil shear modulus of the mixture [N/m^2]
G_0	Soil shear modulus in unfrozen state [N/m^2]
K	Soil bulk modulus of the mixture [N/m^2]
K_w	Water bulk modulus [N/m^2]
L	Latent heat of fusion for water [J/kg]
M	Slope of the critical state line [-]
Q_1	Plastic potential function [-]
S_{ice}	Ice saturation [-]
S_{uw}	Unfrozen water saturation [-]
SSA	Specific surface area [m^2/gr]
T	Current temperature [K]
T_f	Freezing/melting temperature [K]
$T_{f,bulk}$	Freezing/melting temperature of bulk water [K]
T_{ref}	Reference temperature [K]
T_t	Vapour-liquid-solid triple point temperature [K]
Y_{ref}	Reference coordinate for $\left(p^*_{y0}\right)_{in}$ with depth [m]

GREEK SYMBOLS

$\alpha_{x,y,z}$	Thermal expansion coefficient in x, y, z directions [1/K]
α	Parameter for the pressure dependency of ice thawing temperature [-]
β	Parameter controlling the rate of change in soil stiffness with suction [m^2/N]
γ	Plastic potential parameter [-]
γ_w	Unit weight of water [N/m^3]
$d\epsilon$	Increment of strain [-]
$d\epsilon^m$	Increment of strain due to solid phase stress variation [-]
$d\epsilon^{me}$	Increment of elastic strain due to solid phase stress variation [-]
$d\epsilon^{mp}$	Increment of plastic strain due to solid phase stress variation [-]
$d\epsilon^p$	Increment of plastic strain [-]
$d\epsilon^s$	Increment of strain due to suction variation [-]
$d\epsilon^{se}$	Increment of elastic strain due to suction variation [-]
$d\epsilon^{sp}$	Increment of plastic strain due to suction variation [-]
$d\epsilon^e_q$	Increment of elastic shear strain [-]
$d\epsilon^e_v$	Increment of elastic volumetric strain [-]
θ_{ice}	Volumetric ice content [-]
θ_s	Volumetric water content of a saturated soil [-]
θ_{uw}	Volumetric unfrozen water content [-]
θ_w	Volumetric water content [-]
κ	Elastic compressibility coefficient of the soil mixture [-]
κ_s	Elastic compressibility coefficient for suction variation [-]

κ_0	Unfrozen soil elastic compressibility coefficient [-]
λ	Elasto-plastic compressibility coefficient for a frozen state [-]
λ_0	Elasto-plastic compressibility coefficient for unfrozen state [-]
$d\lambda_1$	Plastic multiplier regarding the loading-collapse yield surface [-]
$d\lambda_2$	Plastic multiplier regarding the grain segregation yield surface [-]
λ_r	Parameter for fitting unfrozen water saturation curve [-]
λ_s	Elasto-plastic compressibility coefficient for suction variation [-]
λ_{s1}	Thermal conductivity [W/(mK)]
ν	Specific volume [-]
ν_f	Frozen Soil Poisson's ratio [-]
ρ_b	Dry bulk density of the unfrozen soil [kg/m^3]
ρ_r	Parameter for fitting unfrozen water saturation curve [N/m^2]
ρ_s	Density of the solid material [kg/m^3]
ρ_{ice}	Density of ice [kg/m^3]
ρ_w	Density of water [kg/m^3]
σ	Net stress [N/m^2]
σ^*	Solid phase stress [N/m^2]
ϕ	Residual or critical angle of friction [°]

1 INTRODUCTION

The Frozen and Unfrozen Soil model constitutes a soil model implemented in PLAXIS, capable of describing the mechanical behaviour of frozen soils as a function of temperature, up to the unfrozen state and vice versa. The present constitutive model is the result of a collaboration between the Norwegian University of Science and Technology (NTNU) and Plaxis bv. The aim of this model is to provide a reliable design tool to evaluate the influence of climate/temperature changes in a variety of engineering problems. The increase of engineering activities in cold regions, projects involving artificial ground freezing and consequences of global warming lead to geotechnical applications which deal with frozen/unfrozen ground.

The model is implemented as a user-defined soil model (UDSM) in PLAXIS. Prior to using this model, the 'frozen_soil.dll' and the 'frozen_soil64.dll' should be placed in the sub-folder 'udsm' of the folder where PLAXIS 2D has been saved. The *User-defined* option should be selected through the *Material model* combo box in the *General* tabsheet of the *Material sets* window. In the *Parameters* tabsheet, the 'frozen_soil64.dll' (or 'frozen_soil64.dll') should be selected as the *DLL file* from the drop-down menu. The 'Frozen Soil Model' is used as the *Model in DLL*.

The reader may refer to Chapter 14 of the PLAXIS Material Models Manual for further study on the use of user-defined soil models.

In this document, all relevant symbols adopted in the constitutive model are presented in the list of symbols prior to this Introduction, while the model is outlined in Chapter 2. Physical meaning and determination of the model parameters are discussed in Section 2.7. Verification tests and boundary value problems are used to demonstrate the model's performance capacity, presented in Chapter 3. Conclusions are drawn in Chapter 4.

1.1 UNITS

At the start of the input of a geometry in PLAXIS, a suitable set of basic units should be selected. The basic units comprise a unit for length, force, time, temperature, energy, power and mass. These basic units are defined in the *Model tabsheet* of the *Project properties* window in the Input program. For the use of the present constitutive model specifically, S.I. units are needed. Thus the default PLAXIS units should be changed as follows by the user at the inception of every new project:

Length:	m
Force:	N
Time:	s
Temperature:	K
Energy:	J
Power:	W
Mass:	kg

2 THE CONSTITUTIVE MODEL

The Elastic-Plastic Frozen/Unfrozen Soil model has been originally developed by Amiri, Grimstad, Kadivar & Nordal (2016) and implemented as a user-defined model in PLAXIS after some modifications (Aukenthaler, 2016). The model is developed for simulating the mechanical response of frozen soil under different loading conditions, and also for predicting its deformation under variation of temperature in freezing/thawing periods. It is formulated within the framework of two-stress state variables, using the solid phase stress and cryogenic suction. The solid phase stress is defined as the combined stress in the soil grains and ice, given by Eq. (2.1), in which I denotes the unit tensor (compression is negative).

$$\sigma^* = \sigma - S_{uw} p_w I \tag{2.1}$$

According to this formulation the saturated frozen soil can be viewed as a porous material composed of soil grains and ice in which the pores are filled with water. Ice is part of the solid phase stress because it is able to bear shear stresses. This kind of effective stress based formulation is a Bishop single effective stress, which involves the unfrozen water saturation S_{uw} as the effective stress parameter or Bishop's parameter. The solid phase stress is able to reflect the effect of unfrozen water on the mechanical behaviour. The cryogenic suction, used as the second state variable, allows to build a complete hydro-mechanical framework. By considering the cryogenic suction, it is possible to take the effects of ice content and temperature variation into account.

The cryogenic suction s_c is defined as the pressure difference between ice and liquid water phases, which can be calculated using the Clausius-Clapeyron Eq. (2.2) (Thomas, Cleall, Li, Harris & Kern-Luetschg, 2009). Water pressure p_w and ice pressure p_{ice} are negative.

$$s_c = p_w - p_{ice} \approx -\rho_{ice} L \frac{T}{T_f} \tag{2.2}$$

Hint: Note that following the convention system commonly adopted in thermodynamics, ice and water pressure are positive. However, in this document, the ice and water pressure are negative, in accordance to the commonly used sign convention in solid mechanics and PLAXIS.

2.1 STRAIN DECOMPOSITION

In this model, any strain increment $d\epsilon$, is additively decomposed into the parts given by Eq. (2.3).

$$d\epsilon = d\epsilon^{me} + d\epsilon^{se} + d\epsilon^{mp} + d\epsilon^{sp} \tag{2.3}$$

2.2 ELASTIC RESPONSE

The elastic part of strain due to the solid phase stress variation can be calculated based on the equivalent elastic parameters of the mixture, given by Eqs. (2.4) and (2.5).

$$G = (1 - S_i)G_0 + \frac{S_i E_f}{2(1 + \nu_f)} \tag{2.4}$$

$$K = -(1 - S_i)\frac{(1 + e)p^*_{y0}}{\kappa_0} + \frac{S_i E_f}{3(1 - 2\nu_f)} \tag{2.5}$$

Considering the temperature-dependent behaviour of ice, the following expression is adopted for E_f:

$$E_f = E_{f,ref} - E_{f,inc}(T - T_{ref}) \tag{2.6}$$

The elastic part of strain due to suction variation is calculated by Eq. (2.7), in which I denotes the unit tensor.

$$d\epsilon^{se} = -\frac{\kappa_s}{3(1 + e)}\frac{dS}{S - p_{at}}I \tag{2.7}$$

2.3 YIELD SURFACES

For consistency, when the value of cryogenic suction s_c becomes zero, the model should reduce to a common unfrozen soil model. In accordance with the aim of simplicity, the Modified Cam-Clay model is adopted for the unfrozen state.

For the frozen state, the loading collapse (LC) yield surface is defined as a function of the cryogenic suction s_c and the unfrozen water saturation S_{uw}. The yield criterion due to variation of solid phase F_1 is given by Eq. (2.8).

$$F_1 = (p^* - k_t s_c)\left[(p^* - k_t s_c)S^m_{uw} - \left(p^*_y - k_t s_c\right)\right] + \left(\frac{q^*}{M}\right)^2 \tag{2.8}$$

in which

$$p^*_y = p^*_c\left(\frac{p^*_{y0}}{p^*_c}\right)^{\frac{\lambda_0 - \kappa}{\lambda - \kappa}} \tag{2.9}$$

$$\lambda = \lambda_0[(1 - r)\exp(-\beta s_c) + r] \tag{2.10}$$

$$\kappa = -\frac{1 + e}{K}p^*_{y0} \tag{2.11}$$

To simulate ice segregation phenomenon, the grain segregation (GS) yield criterion is adopted for suction induced plastic deformation and Eq. (2.12) applies.

$$F_2 = s_c - s_{c,seg} = 0 \tag{2.12}$$

Figure 2.1 illustrates the complete yield surface of the model in p^*-q^*-s_c space for $m = 0$.

Figure 2.2 depicts the influence of the yield parameter m on the shape of the yield surface in p^*-q^* plane at a constant value of S_{uw} = 0.01.

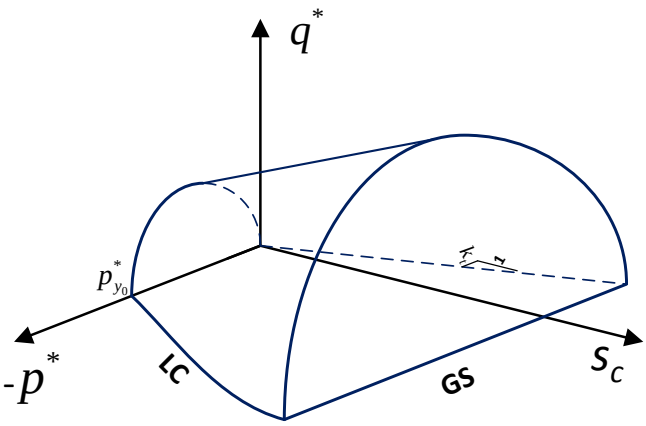

Figure 2.1 Three-dimesnional view of the yield surface in p^*-q^*-s_c space for m = 0

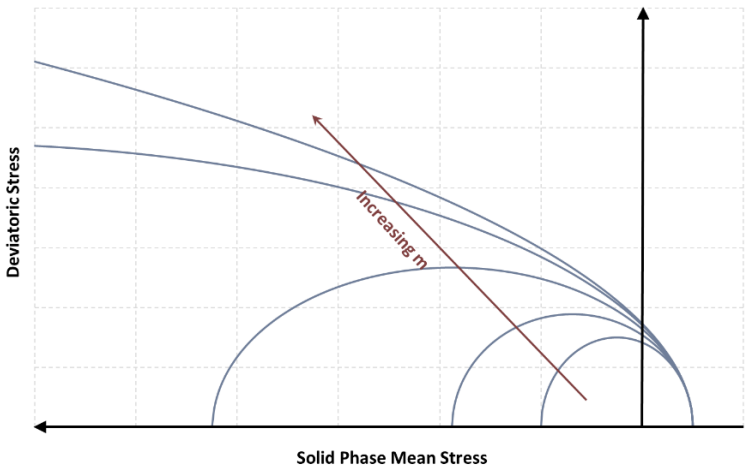

Figure 2.2 Influence of the yield parameter m in the shape of the yield surface in p^*-q^* plane for S_{uw} = 0.01

2.4 HARDENING RULES

A plastic compression due to the variation of solid phase stress results in stiffer behaviour of the soil and causes the LC yield surface to move outward. Furthermore, this plastic compression results in a decrease in the dimensions of voids, hence, lower segregation threshold value is expected. This behaviour could be captured by a coupled hardening

rule (Eq. (2.13)), which causes the GS yield surface to shift downward.

$$\frac{dp^*_{y0}}{p^*_{y0}} = -\frac{1+e}{\lambda_0 - \kappa_0} d\epsilon_v^{mp} - \frac{1+e}{\lambda_0 - \kappa_0} d\epsilon_v^{sp} \tag{2.13}$$

Figure 2.3 shows a typical evolution of the yield surfaces due to plastic compression in p^*-s_c (a) and p^*-q^* (b) planes.

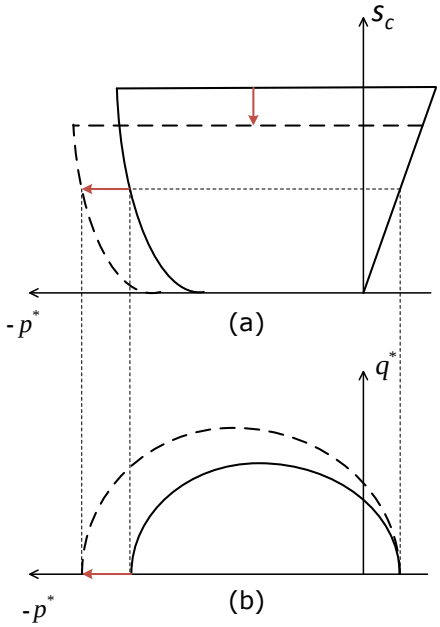

Figure 2.3 Evolution of yield surfaces due to plastic compression in p^*-s_c (a) and p^*-q^* (b) planes

A plastic dilation due to occurrence of ice segregation causes the GS yield surface to move upward. This plastic dilation results in softer behaviour of the soil, hence, an inward movement of the LC yield surface should also be considered, given by Eq. (2.14).

$$\frac{ds_{c,seg}}{s_{c,seg} + p_{at}} = \frac{1+e}{S_{uw}(\lambda_s + \kappa_s)} d\epsilon_v^{sp} + \frac{1+e}{\lambda_s + \kappa_s}\left(1 - \frac{s_c}{s_{c,seg}}\right) d\epsilon_v^{mp} \tag{2.14}$$

Figure 2.4 shows a typical evolution of the yield surfaces due to ice segregation phenomenon in p^*-s_c (a) and p^*-q^* (b) planes.

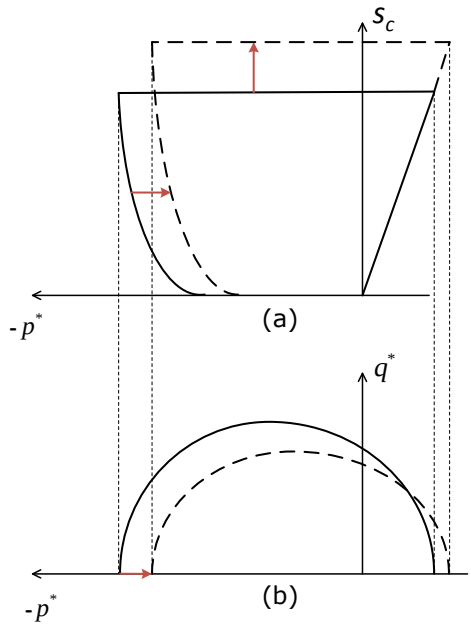

Figure 2.4 Evolution of yield surfaces due to ice segregation phenomenon in p^*-s_c (a) and p^*-q^* (b) planes

2.5 FLOW RULES

A non-associated flow rule is used for the LC yield surface (Eq. (2.15)), while an associated flow rule is employed for the GS yield surface (Eq. (2.16)). The plastic potential function Q_1 is given by Eq. (2.17).

$$d\epsilon^{mp} = d\lambda_1 \frac{\partial Q_1}{\partial \sigma^*} \tag{2.15}$$

$$d\epsilon^{sp} = d\lambda_2 \frac{\partial F_2}{\partial s_c} I \tag{2.16}$$

$$Q_1 = S_{uw}^{\gamma} \left(p^* - \frac{p_y^* + k_t s_c}{2} \right)^2 + \left(\frac{q^*}{M} \right)^2 \tag{2.17}$$

2.6 FREEZING/THAWING TEMPERATURE AND UNFROZEN WATER SATURATION

In this Section two approaches are presented in order to estimate the freezing/thawing temperature T_f and the unfrozen water saturation S_{uw}.

- In the approach adopted by Amiri, Grimstad, Kadivar & Nordal (2016), the freezing/thawing temperature at a given ice pressure is calculated by Eq. (2.18), in which p_{ref} and α are two constant parameters (commonly $7 \leq \alpha \leq 9$, p_{ref} = -395

MPa, T_{ref} = 273.16 K).

$$T_f = T_{ref}\left(\frac{p_{ice}}{-p_{ref}} + 1\right)^{\frac{1}{\alpha}} \tag{2.18}$$

The unfrozen water saturation S_{uw} in PLAXIS is calculated based on Eq. (2.19) (Nishimura, Gens, Olivella & Jardine, 2009), in which ρ_r and λ_r are two constants.

$$S_{uw} = \left[1 + \left(\frac{s_c}{\rho_r}\right)\frac{1}{1-\lambda_r}\right]^{-\lambda_r} \tag{2.19}$$

- In the approach developed by Aukenthaler, Brinkgreve & Haxaire (2016), a different formulation is adopted. The pressure dependence of the melting temperature for ice is expressed according to Wagner, Riethmann, Feistel & Harvey (2011) by Eq. (2.20), in which T_t equals 273.16 K and p_t equals -611.657 Pa. The coefficients a_i and the exponents b_i are given in Table 2.1.

$$\frac{p_{melt}}{p_t} = 1 + \sum_{i=1}^{3} a_i\left[1 - \left(\frac{T}{T_t}\right)^{b_i}\right] \tag{2.20}$$

Table 2.1 Coefficients a_i and exponents b_i (Wagner, Riethmann, Feistel & Harvey, 2011)

i	a_i	b_i
1	0.119539337×10^7	0.300000×10^1
2	0.808183159×10^5	0.257500×10^2
3	0.333826860×10^4	0.103750×10^3

The contribution of pore water pressure p_w and cryogenic suction s_c results in ice pressure:

$$p_{ice} = p_w - s_c \tag{2.21}$$

By substituting Eq. (2.21) into Eq. (2.20), Eq. (2.22) is obtained.

$$\frac{p_w - s_c}{-611.657Pa} = 1 + \sum_{i=1}^{3} a_i\left[1 - \left(\frac{T_f}{273.16K}\right)^{b_i}\right] \tag{2.22}$$

The unfrozen water saturation S_{uw} is related to the volumetric unfrozen water content θ_{uw} by Eq. (2.23). The latter is related to the temperature by using an empirical formulation based on the results of Anderson & Tice (1972). Eq. (2.24) gives the empirical relationship and it is only valid for $T \leq T_{f,bulk}$.

$$S_{uw} = \frac{\theta_{uw}}{n} \tag{2.23}$$

$$\theta_{uw} = \frac{\rho_w}{\rho_b}\exp\left(0.2618 + 0.5519\ln(SSA) - 1.4495(SSA)^{-0.2640}\ln|T|\right) \tag{2.24}$$

with

$$|T| = T_{f,bulk} - T \tag{2.25}$$

In Eq. (2.25), $T_{f,bulk}$ refers to the bulk freezing point (273.16 K) and T to the actual temperature in Kelvin.

To use Eq. (2.24) properly, θ_{uw} should not exceed the volumetric water content of a fully saturated soil, which equals the porosity of the soil. This cut-off value is necessary because Eq. (2.24) is empirical and provides values of θ_{uw} bigger than θ_{sat} at temperatures close to $T_{f,bulk}$. An important assumption is that the cut-off point can be seen as the freezing/thawing temperature T_f of a soil-water system where pore water pressure equals zero. In other words, T_f obtained from the equation proposed by Anderson & Tice (1972) is the soil-type dependent freezing/thawing temperature (Aukenthaler, Brinkgreve & Haxaire, 2016).

The specific surface area (SSA) of soil is estimated based on the empirical power pedo-transfer function, given by Eq. (2.26). Based on Fooladmand (2011), Eq. (2.26) is found to give good approximation of the specific surface area of soils.

$$SSA = 3.89 d_g^{-0.905} \tag{2.26}$$

The geometric mean particle diameter d_g is defined by Eq. (2.27) (Shirazi & Boersma, 1984), based on the U.S.D.A. classification scheme of soil (Table 2.2). In Eq. (2.27), the arithmetic means are given by d_{clay} = 0.001 mm, d_{silt} = 0.026 mm and d_{sand} = 1.025 mm.

$$d_g = \exp\left(\sum_{i=1}^{3} m_i \ln d_i\right) \tag{2.27}$$

Table 2.2 U.S.D.A. clasification scheme

clay		d <	0.002	mm
silt	0.002	≤ d <	0.05	mm
sand	0.05	≤ d <	2.0	mm

2.7 INPUT PARAMETERS AND STATE VARIABLES

There are three kinds of input parameters in this model: the soil parameters, the parameters for initialising the state variables and the ice and water parameters. They are summarised in Table 2.3. The description and S.I. units used for these parameters are presented in Chapter .

Table 2.3 Input model parameters

Soil parameters	T_{ref}	$E_{f,ref}$	$E_{f,inc}$	ν_f	G_0	κ_0	p_c^*	λ_0		
	γ	k_t	M	λ_s	κ_s	r	β	m	p_{at}	
Parameters for initialising the state variables	$\left(p_{y0}^*\right)_{in}$	λ_r	Y_{ref}	Δp_{y0}^*	e_0	$(s_{c,seg})_{in}$				
Ice and water parameters	ρ_r	α	T_{ref}	p_{ref}	K_w					

- In the approach adopted by Amiri, Grimstad, Kadivar & Nordal (2016), the main extracting method of the parameters is by fitting the experimental curves from element tests. Plotting the results of an isotropic drained compression test for an unfrozen state of the soil in ν:ln p plane can provide the data to find the elastic compressibility coefficient κ_0, the reference stress p_c^*, the elastic-plastic compressibility coefficient λ_0 and the initial value of the pre-consolidation stress

$\left(p^*_{y0}\right)_{in}$ at Y_{ref}. It should be noted that the pre-consolidation stress is depth-dependent and the following expression (Eq. (2.28)) is considered for determination of its value with depth.

$$\begin{aligned} \left(p^*_{y0}\right)_Y &= \left(p^*_{y0}\right)_{Y_{ref}} \quad \text{if} \quad Y \geq Y_{ref} \\ \left(p^*_{y0}\right)_Y &= \left(p^*_{y0}\right)_{Y_{ref}} + \Delta p^*_{y0}\left(Y_{ref} - Y\right) \quad \text{if} \quad Y < Y_{ref} \end{aligned} \tag{2.28}$$

A drained simple shear strength test at an unfrozen state of the soil can be used to determine the elastic shear modulus of the soil in unfrozen state G_0 and the slope of the critical state line M.

Conducting an unconfined triaxial compression test in an arbitrary reference temperature at a frozen state of the soil, can be used for determining the reference Young's modulus of the frozen soil $E_{f,ref}$. Similar test in a different negative temperature can be considered to find $E_{f,inc}$. Then, an isotropic compression test at a frozen state of the soil with a certain value of ice saturation can be used for calculating the Poisson's ratio of the soil in the fully frozen state ν_f, using Eq. (2.5).

Considering Eq. (2.10), β and r can be calculated by determining λ at two different frozen states of the soil. The parameters k_t and m can be determined based on the results of drained shear stress tests at two different frozen states of the soil using Eq. (2.29).

$$q^*_f = M\sqrt{2 - S^m_{uw}}\left(p^*_f + k_t s_c\right) \tag{2.29}$$

The plastic potential parameter γ can be found using a trial-and-error procedure to fit the volumetric behaviour of the soil at two different frozen states. Finally, the result of a test involving a freezing-thawing cycle plotted in ν:ln$(s_c + p_{at})$ plane is required to determine the values of $\left(s_{c,seg}\right)_{in}$, λ_s and κ_s.

- The approach adopted by Aukenthaler, Brinkgreve & Haxaire (2016) is slightly different. Table 2.4 presents the suggested soil tests and the parameters determined by each one of them.

Table 2.4 Model parameters determination suggested by Aukenthaler, Brinkgreve & Haxaire (2016)

Type of laboratory test	Model parameters to determine the state variables
Oedometer tests (or isotropic compression tests) in unfrozen and frozen state	The ν:ln p plane provides data to find the parameters $\left(p^*_{y0}\right)_{in}$, furthermore the parameters β, κ_0, r and p^*_c can be determined either by the sequential calibration procedure proposed by Onza & Wheeler (2010) (isotropic compression tests) or by the approach of Zhang, Alonso & Casini (2016) (temperature-controlled oedometer tests). The latter is reformulated for the present constitutive model in Aukenthaler (2016). The parameter λ_0 can be obtained by taking the compression index C_c of the oedometer test in an unfrozen state into account ($\lambda_0 = C_c / \ln(10)$)
Simple shear test in unfrozen state	Obtain G_0 and M
Unconfined axial compression test at an arbitrary reference temperature at a frozen state	Determine $E_{f,ref}$ and ν_f
Unconfined axial compression test at a different temperature at a frozen state	Determine $E_{f,inc}$ and k_t
Frost heave test (freezing-thawing cycle)	Obtain $\left(s_{c,seg}\right)_{in}$, λ_s and κ_s by plotting the results in the ν:ln$(s_c + p_{at})$ plane

Aukenthaler, Brinkgreve & Haxaire (2016) also proposed correlations and default values as first estimation of the model parameters. Based on Tsytovich (1975) and Johnston

(1981), Table 2.5 presents values of $E_{f,ref}$ and $E_{f,inc}$ for three different frozen soils. Nevertheless, these values should be used with caution.

Table 2.5 Default values of elastic parameters

Soil parameters	Frozen sand	Frozen silt	Frozen clay
$E_{f,ref}$ (MPa)	500	400	500
$E_{f,inc}$ (MPa/K)	2100	1400	230

The Poisson's ratio of ice ν_{ice} is approximately 0.31. It is proposed to use a value of ν_f close to ν_{ice}. The slope of the critical state line M may be calculated by Eq. (2.30) for triaxial compression (-) and triaxial extension (+). Default values for the residual or critical angle of friction ϕ' are provided by Ortiz, Serra & Oteo (1986).

$$M = \frac{6 \sin \phi'}{3 \pm \sin \phi'} \tag{2.30}$$

The initial threshold value for grain segregation $\left(s_{c,seg}\right)_{in}$ is approximated based on Rempel (2007) by use of Eq. (2.31). This approximation provides reasonable values. The proposed default values when no frost heave test has been performed are 0.55 MPa for sand, 1.25 MPa for silt and 3.50 MPa for clay, respectively.

$$\left(s_{c,seg}\right)_{in} \approx |T_{f,bulk} - T| \times \frac{MPa}{K} \tag{2.31}$$

3 VERIFICATION TESTS AND BOUNDARY VALUE PROBLEMS

In this section, the application of the elastic-plastic frozen and unfrozen soil model is illustrated with some verification example. In the first example (Section 3.1), triaxial tests under different temperatures and confining pressures are simulated to show the behaviour of the model in different conditions. In the second example (Section 3.2), a freezing-thawing cycle is applied on a soil sample to show the capability of the model in representing the frost heave and thawing settlement phenomenon. A chilled pipeline buried in unfrozen ground is then simulated as a more practical application (Section 3.3). More practical applications can also been found in Aukenthaler (2016).

An overview of the parameters selected for each one of the considered tests/applications in this section is presented below, from Table 3.1 to 3.3. S.I. units are used (see Section 1.1).

Table 3.1 Thermal parameters of water and ice phases

Parameter	Triaxial Tests	Freezing-thawing cycle	Chilled pipeline
T_{ref} (K)	272.16	274.16	274.16
γ_{water} (N/m^3)	10^4	10^4	10^4
c_{water} (J/kg/K)	4181	4181	4181
$\lambda_{s1\,water}$ (W/m/K)	0.6	0.6	0.6
L_{water} (J/kg)	334×10^3	334×10^3	334×10^3
α_{water} (1/K)	0.21×10^{-3}	0.21×10^{-3}	0.21×10^{-3}
T_{water} (K)	293.16	274.16	274.16
c_{ice} (J/kg/K)	2108	2108	2108
$\lambda_{s1\,ice}$ (W/m/K)	2.22	2.22	2.22
α_{ice} (1/K)	0.05×10^{-3}	0.05×10^{-3}	0.05×10^{-3}

Table 3.2 Soil properties

Parameter	Triaxial Tests	Freezing-thawing cycle	Chilled pipeline
General tabsheet			
Drainage type	Drained	Drained	Drained
γ_{unsat} (N/m^3)	18×10^3	20×10^3	18×10^3
γ_{sat} (N/m^3)	18×10^3	20×10^3	18×10^3
e_0 (-)	0.3	0.9	0.5
Groundwater tabsheet			
k_x (m/s)	1.396×10^{-6}	0.55×10^{-6}	0.263×10^{-6}
k_y (m/s)	1.396×10^{-6}	0.55×10^{-6}	0.263×10^{-6}
Thermal tabsheet			
c_s (J/kg/K)	2000	945	920
λ_{s1} (W/m/K)	4.0	1.5	2.0
ρ_s (kg/m^3)	2200	2600	2700
α_x (1/K)	5.2×10^{-6}	5.2×10^{-6}	0.052×10^{-3}
α_y (1/K)	5.2×10^{-6}	5.2×10^{-6}	5.2×10^{-6}
α_z (1/K)	5.2×10^{-6}	5.2×10^{-6}	5.2×10^{-6}
Intial tabsheet			
$K_{0,x}$ (-)	1.0	0.9825	1.0
$K_{0,z}$ (-)	1.0	0.9825	1.0

Table 3.3 Frozen/unfrozen material properties

Parameter	Triaxial Tests	Freezing-thawing cycle	Chilled pipeline
Model-ID	15211522	15211522	15211522
T_{ref} (K)	273.16	273.16	273.16
$E_{f,ref}$ (N/m^2)	50×10^6	6×10^6	30×10^6
$E_{f,inc}$ (N/m^2/K)	10×10^6	9.5×10^6	10×10^6
ν_f (-)	0.48	0.35	0.35
G_0 (N/m^2)	5×10^6	2.22×10^6	4.2×10^6
κ_0 (-)	0.3	0.08	0.11
p_c^* (N/m^2)	-470×10^3	-45×10^{-3}	-550×10^3
λ_0 (-)	0.4	0.4	0.4
γ (-)	0.2	1.0	1.0
k_t (-)	0.09	0.06	0.07
M (-)	1.17	0.77	0.97
λ_s (-)	0.4	0.5	0.6
κ_s (-)	8×10^{-3}	5×10^{-3}	0.5×10^{-3}
r (-)	0.59	0.6	0.6
β (m^2/N)	0.09×10^{-6}	0.6×10^{-6}	0.08×10^{-6}
λ_r (-)	0.6	0.18	0.6
ρ_r (N/m^2)	2.4×10^6	8000	2.4×10^6
α (-)	9	9	9
T_{ref} (K)	273.16	273.16	273.16
p_{ref} (N/m^2)	-395×10^6	-395×10^6	-395×10^6
m (-)	0.5	1.0	1.0
p_{y0}^* (N/m^2)	-2.1×10^6	-55×10^3	-800×10^3
Y_{ref} (m)	0.0	0.0	1.75
Δp_{y0}^* (N/m^2/m)	0.0	0.0	-20×10^3
e_0 (-)	0.3	0.9	0.5
$(s_{s,seg})_{in}$ (N/m^2)	8×10^6	1.5×10^6	1.8×10^6
p_{at} (N/m^2)	-100×10^3	-100×10^3	-100×10^3
K_w (N/m^2)	10^9	10^9	10^9

3.1 TRIAXIAL TESTS

In this series of examples, a frozen sandy soil is subjected to a set of triaxial tests under different condition of temperature and confining pressure. Three tests are conducted in constant temperature of -4°C and at different confining pressure of 0.2, 0.6 and 1 MPa. Three other tests are simulated under constant confining pressure of 1 MPa and different temperatures of -1, -2 and -4°C. Results show the capability of the model to reflect the influence of temperature and confining pressure on the behaviour.

Triaxial tests are conducted in PLAXIS 2D. One-fourth of the specimen geometry is modelled, depicted in Figure 3.1. An axisymmetric model with 6-noded triangular elements is used. The *coarse* option is used for the element distribution. Confining pressures are represented by distributed loads on the right and top model boundaries. The axial load is applied using prescribed displacement on the top model boundary.

Since the tests are conducted in drained conditions, *seepage* boundary condition is assigned for the top and right boundaries. Due to symmetry, the left and bottom boundaries are *closed* for flow.

Since the temperature of the sample is considered to be constant during a test, constant temperature condition is specified for the soil body and the right and top boundaries. Similar to hydraulic boundary conditions, the left and bottom boundaries are *closed*.

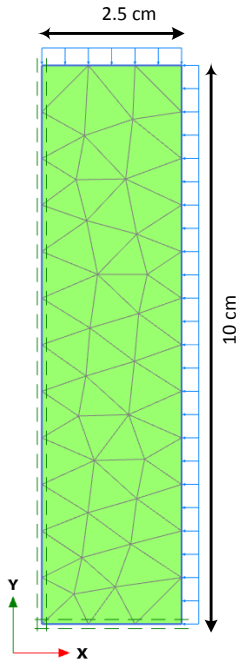

Figure 3.1 Model geometry and generated mesh

The thermal properties of water and ice phases are introduced in the *Constants* tabsheet of the *Project properties* window. The relevant parameters are listed in Table 3.1. The selected soil properties are presented in Table 3.2 and 3.3.

For each triaxial test three calculation phases are considered. Details about the calculation phases are presented in Table 3.4. It should be noted, in case of using the elastic-plastic frozen soil model, the steady state thermal flow calculation type is mandatory in the initial calculation phase to assign an appropriate initial condition for cryogenic suction and unfrozen water saturation.

Table 3.4 Calculation phases for the triaxial tests

Phase	Calculation type	Loading	Pore pressure	Thermal	Time interval (s)
Initial	K0	Staged constr.	Phreatic	Steady-state	-
Confining pressure	Fully coupled	Staged constr.	-	from previous ph.	36×10^3
Shearing	Fully coupled	Staged constr.	-	from previous ph.	100×10^3

Figures 3.2 and 3.3 illustrate the calculated results for the set of triaxial tests conducted at different confining pressure and temperature. The graph represent the evolution of deviatoric stress over axial strain as well as the volumetric behaviour with axial strain. The following objective features are addressed:

- In the elastic zone, the stiffness increases with decreasing temperature.
- With decreasing temperature and/or increasing confining pressure the strength increases.
- Hardening and softening behaviour, as well as the associated compressive and dilative behaviour can be represented.

- The volumetric deformation is significantly affected by the confining pressure. The volume reduces with the increase in axial strain under high confining pressures. At low confining pressures the volume always reduces to a critical value, before volume expansion in the strain softening stage takes place.

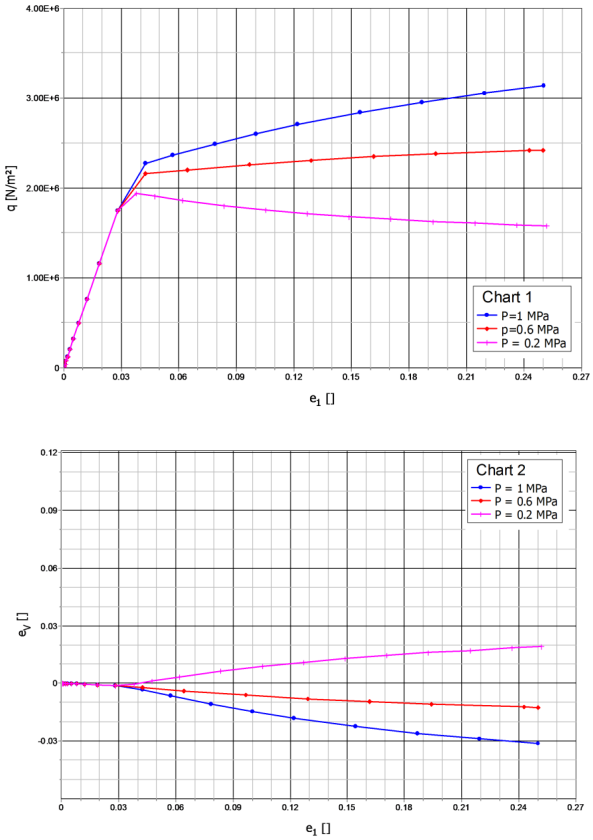

Figure 3.2 Results of the triaxial tests at different confining pressures and constant temperature of -4°C (for a Gauss point at the center of the model)

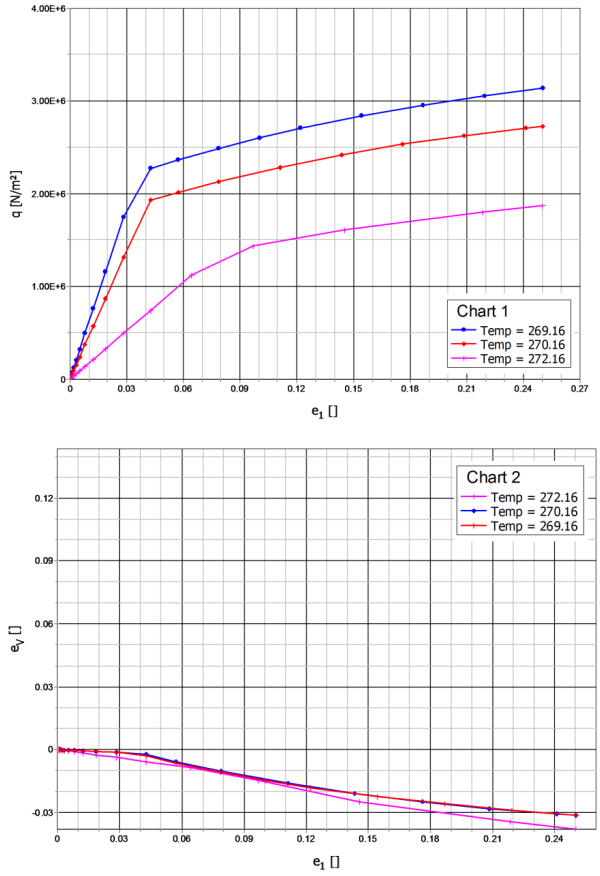

Figure 3.3 Results of the triaxial tests at different temperatures and constant confining pressure of 1 MPa (for a Gauss point at the center of the model)

3.2 FREEZING-THAWING CYCLE

In this example, a frozen soil sample is subjected to a cycle of freezing and thawing. This example shows the ability of the model to simulate the ice segregation phenomenon (frost heave) as well as the thaw settlement behaviour. With this application the coupling of the grain segregation (GS) yield surface with the loading collapse (LC) yield surface is demonstrated.

The model geometry is depicted in Figure 3.1. A confining pressure of 90 kPa is applied by distributed load on the right and top model boundaries. Temperature variation over time, given by Eq. (3.1), is applied on the same boundaries. Eq. (3.1) is presented graphically in Figure 3.4. Seepage boundary condition is assigned for the top and right boundaries. Due to symmetry the left and bottom boundaries are closed for flow and temperature.

$$T = 1 - 5\sin\left(\frac{2\pi}{14400}t\right) \tag{3.1}$$

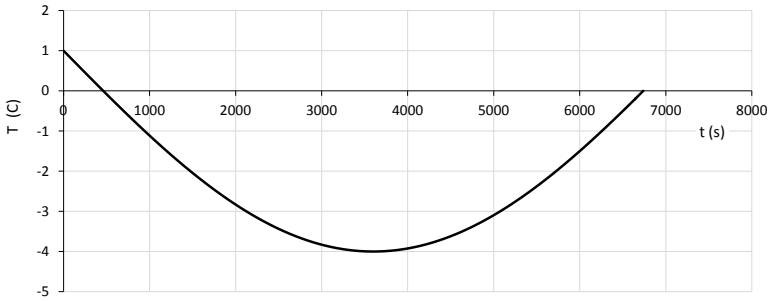

Figure 3.4 Temperature variation over time

The adopted project and material properties are presented in Table 3.1 to 3.3. Three calculation phases are considered. Details about the calculation phases are presented in Table 3.5. The *Ignore suction* option is unselected for all phases. During thermal loading (third calculation phase), special attention is required to set the controlling parameters of the numerical solution. The *Max steps* option is set to 10000 (for both Numerical and Flow control parameters), the *Tolerated error* is set equal to 0.005 (for both Numerical and Flow control parameters), the *Max load fraction per step* is set to 0.1, the *Over-relaxation factor* is set to 0.8 (for both Numerical and Flow control parameters). It is generally recommended for the latter to be less than 1.

Table 3.5 Calculation phases for the triaxial tests

Phase	Calculation type	Loading	Pore pressure	Thermal	Time interval (s)
Initial	K0	Staged constr.	Phreatic	Steady-state	-
Confining pressure	Fully coupled	Staged constr.	-	from previous ph.	36×10^3
Freezing-thawing cycle	Fully coupled	Staged constr.	-	from previous ph.	6800

Figure 3.5 illustrates the volumetric deformation of the sample during the freezing-thawing cycle. During the first stage of the cooling process, the elastic regime (κ_s) dominates the behaviour by bonding the grains together. This results in a decrease in the volume of the specimen. Continuing the cooling process, the cryogenic suction s_c will hit the GS yield surface and the ice segregation phenomenon will start. This results in a significant increase in the volume of the soil (frost heave). Additionally, the LC yield curve moves inward and the pre-consolidation stress decreases. Upon thawing, the LC yield curve is hit and plastic compression as well as thawing consolidation will occur (thawing settlement).

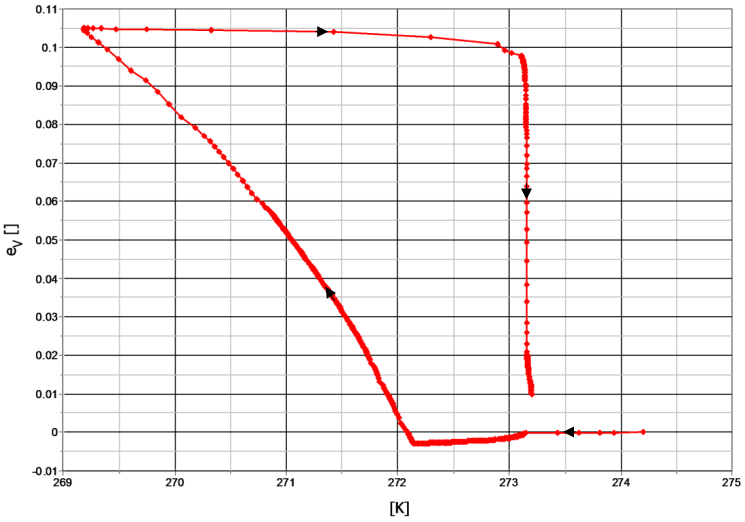

Figure 3.5 Temperature variation over time

3.3 CHILLED PIPELINE

A buried chilled pipeline causes the temperature of its surrounding ground to decrease. Upon freezing, soil will expand not only due to the expansion of water but also because of water migration and formation of ice lenses. Frost heave is an anticipated issue in the design of this kind of pipelines. In this example, a gas pipeline with a diameter of 273 mm and temperature of -4°C is considered to be buried in saturated silt, and the goal is to simulate its effects on the surrounding ground.

A plane-strain model with 6-noded elements is considered in PLAXIS 2D. Due to symmetry, only half of the geometer is modelled, displayed in Figure 3.6. The soil is fully saturated and the water table is located at the ground level. The top and bottom boundaries are drained and their temperature is set to +1°C and +4°C respectively. The right boundary is also drained and its temperature is determined by the steady state thermal analysis of the field (Initial calculation phase). Due to symmetry, the left boundary is undrained and adiabatic. The initial ground temperature is also determined by the steady state thermal analysis (Initial calculation phase).

The adopted project and material properties are presented in Table 3.1 to 3.3. To simulate the pipeline, *Plate* elements are used with bending stiffness EI equal to 282×10^3 Nm^2/m.

Four calculation phases are considered. Details about the calculation phases are presented in Table 3.6. In the Initial phase, the steady-state thermal flow is considered to determine the initial ground temperature and assign the temperature condition of the right boundary for the next calculation phases. For the 'Pipe installation' phase, it is assumed that a trenchless method is used for pipe installation. In the 'Cooling down' phase, it is assumed that it takes 10 days until the pipeline cools down to -4°C. A linear function for this cooling period is considered for the pipeline. In the 'Time effect' phase, pipe temperature stays constant at -4°C and the temperature field, ice saturation and soil deformation are calculated for the next 100 days.

The *Ignore suction* option is unselected for all phases. The following numerical settings

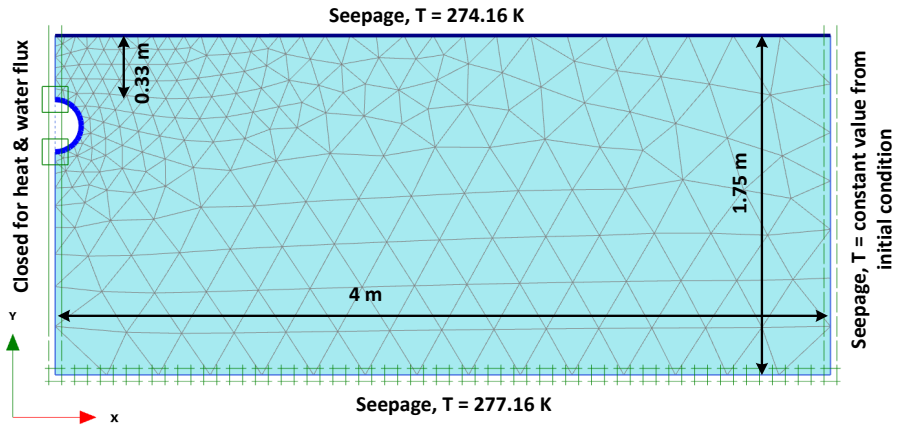

Figure 3.6 Model geometry, generated mesh and boundary conditions for the chilled pipeline

apply for both 'Cooling down' and 'Time effect' phases. The *Max steps* option is set to 10000 (for both Numerical and Flow control parameters), the *Max time step* is set equal to 36×10^3, the *Tolerated error* is set equal to 0.0005 (for both Numerical and Flow control parameters), the *Max load fraction per step* is set to 0.001, the *Over-relaxation factor* is set to 0.8 (for both Numerical and Flow control parameters).

Table 3.6 Calculation phases for the triaxial tests

Phase	Calculation type	Loading	Pore pressure	Thermal	Time interval (s)
Initial	K0	Staged constr.	Phreatic	Steady-state	-
Pipe installation	Fully coupled	Staged constr.	-	from previous ph.	86.4×10^3
Cooling down	Fully coupled	Staged constr.	-	from previous ph.	864×10^3
Time effect	Fully coupled	Staged constr.	-	from previous ph.	8.64×10^3

The temperature field and ice saturation profile after the third and fourth calculation phases are presented in Figures 3.7 and 3.8 respectively. Freezing is initiated around the pipeline and penetrates through the ground. Some unfrozen water still remains in frozen areas, which is essential for frost heave to take place. A total heave of about 2.7 cm is observed at the centerline of the pipe. Figure 3.9 shows the deformed mesh of the model after 110 days. The heave is actually attributed to migration of water and the simulation results are in agreement with this hypothesis. Figure 3.10 presents the vectors of ground water flow after the first 10 days. As expected, water is moving to the freezing front.

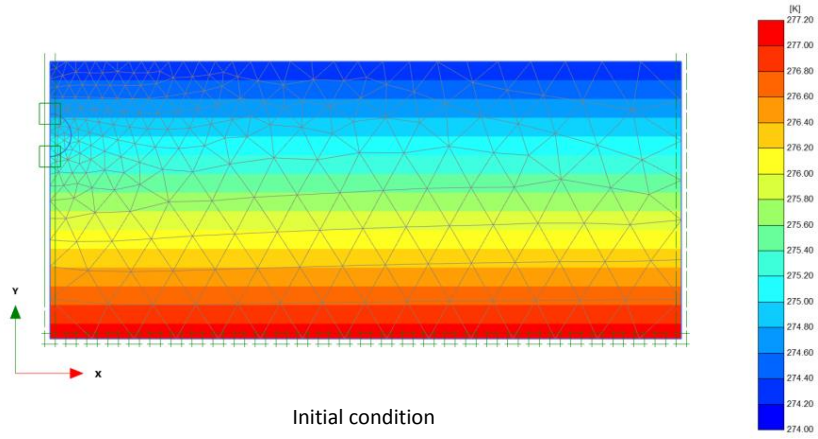

Initial condition

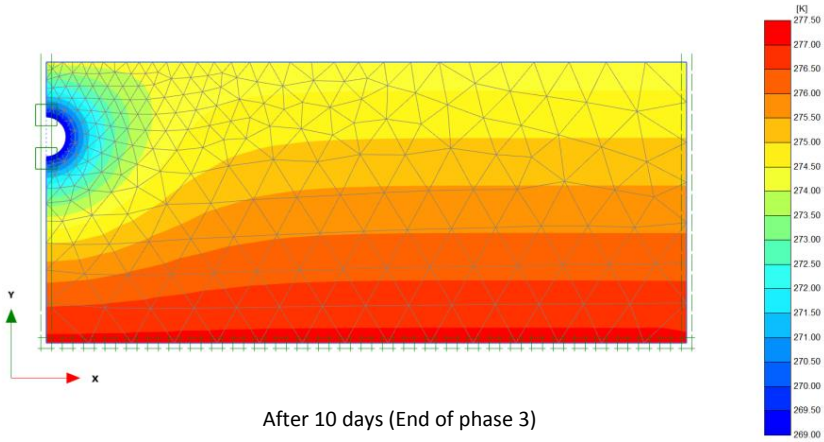

After 10 days (End of phase 3)

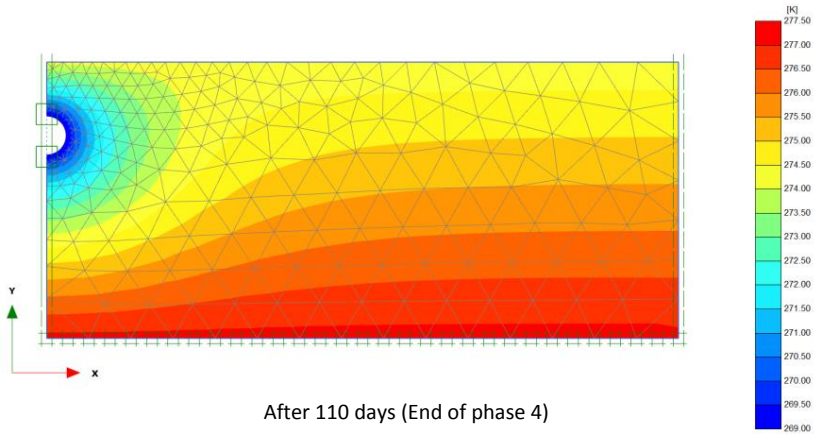

After 110 days (End of phase 4)

Figure 3.7 Temperature profiles

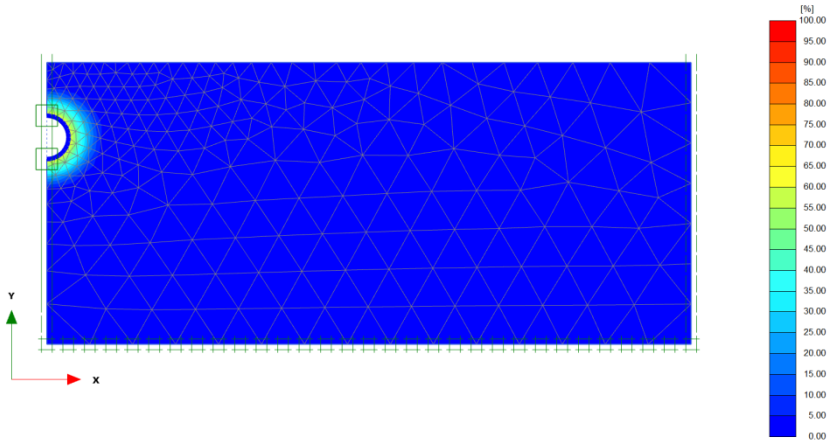

After 10 days (End of phase 3)

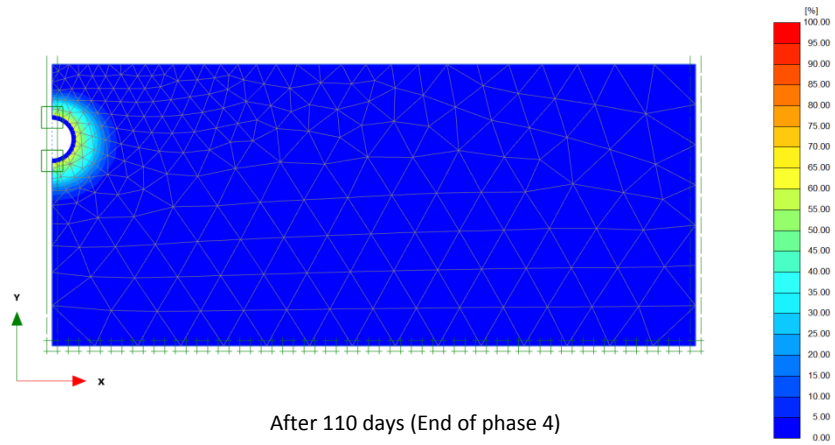

After 110 days (End of phase 4)

Figure 3.8 Ice saturation profiles

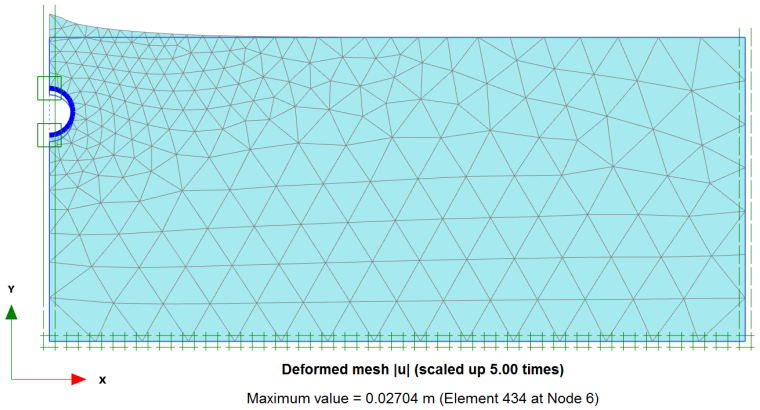

Figure 3.9 Frost heave after 110 days

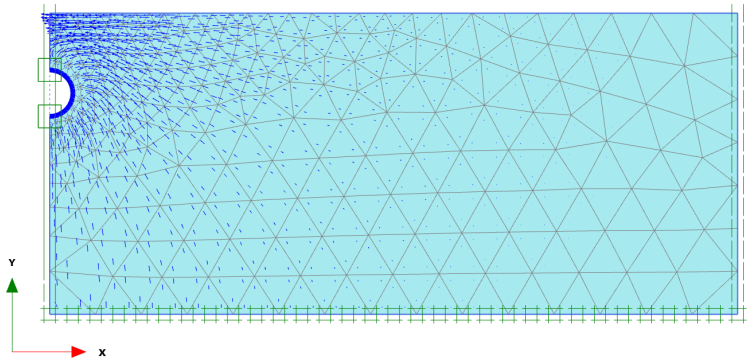

Figure 3.10 Water migration to frost front (after 10 days)

4 CONCLUSIONS

The constitutive model developed by Amiri, Grimstad, Kadivar & Nordal (2016) characterises the mechanical behaviour of frozen soils as a function of temperature, up to the unfrozen state and vice versa. The model is implemented as a user-defined soil model (UDSM) in PLAXIS, using the fully coupled *THM* calculation options (Aukenthaler, 2016). A variety of geotechnical problems which include freezing and thawing soils can be studied via this constitutive model. More precisely, the dependence of stiffness and shear strength on temperature, frost heave and thaw settlements can be captured by the model.

An overview of the model parameters together with suggestions upon essential laboratory testing for their determination are presented in this document. Both approaches adopted by Amiri, Grimstad, Kadivar & Nordal (2016) and Aukenthaler, Brinkgreve & Haxaire (2016) are discussed. Empirical relationships and default values for certain parameters are discussed as well.

A set of verification examples and one characteristic application are presented. The capabilities of the model are demonstrated successfully.

5 REFERENCES

[1] Amiri, S.A.G., Grimstad, G., Kadivar, M., Nordal, S. (2016). A constitutive model for rate-independent behavior of saturated frozen soils. Canadian Geotechnical Journal, 53(10), 1646–1657.

[2] Anderson, D.M., Tice, A.R. (1972). Predicting unfrozen water contents in frozen soils from surface area measurements. Highway Research Record, (393), 12–18.

[3] Aukenthaler, M. (2016). The Frozen & Unfrozen Barcelona Basic Model, verification and validation of a new constitutive model. Master's thesis, Delft University of Technology, the Netherlands.

[4] Aukenthaler, M., Brinkgreve, R.B.J., Haxaire, A. (2016a). Evaluation and application of a constitutive model for frozen and unfrozen soil. In Proceedings GeoVancouver 2016. Vancouver BC, Canada, 3668.

[5] Aukenthaler, M., Brinkgreve, R.B.J., Haxaire, A. (2016b). A practical approach to obtain the soil freezing characteristic curve and the freezing/melting point of a soil-water system. In Proceedings GeoVancouver 2016. Vancouver BC, Canada, 3821.

[6] Fooladmand, H.R. (2011). Estimating soil specific surface area using the summation of the number of spherical particles and geometric mean particle-size diameter. African Journal of Agricultural Research, 6(7), 1758–1762.

[7] Johnston, G.H. (1981). Permafrost Engineering Design and Construction. Toronto: Wiley.

[8] Nishimura, S., Gens, A., Olivella, S., Jardine, R.J. (2009). Thm-coupled finite element analysis of frozen soil: formulation and application. Géotechnique, 59(3), 159–171.

[9] Onza, D.G.A.F.D., Wheeler, S.J. (2010). A sequential method for selecting parameter values in the barcelona basic model. Canadian Geotechnical Journal, 47(11), 1175–1186.

[10] Ortiz, J., Serra, J., Oteo, C. (1986). Curso Aplicado de Cimentaciones (third edition). Madrid: Colegio de Arquitectos de Madrid.

[11] Rempel, A.W. (2007). Formation of ice lenses and frost heave. Journal of Geophysical Research: Earth Surface, 112(F2).

[12] Shirazi, M.A., Boersma, L. (1984). A unifying quantitative analysis of soil texture. Soil Science Society of America Journal, 48(1), 142–147.

[13] Thomas, H.R., Cleall, P.J., Li, Y., Harris, C., Kern-Luetschg, M. (2009). Modelling of cryogenic processes in permafrost and seasonally frozen soils. Géotechnique, 59(3), 173–184.

[14] Tsytovich, N.A. (1975). Mechanics of frozen ground (trans.). Washington: Scripta Book Co.

[15] Wagner, W., Riethmann, T., Feistel, R., Harvey, A.H. (2011). New equations for the sublimation pressure and melting pressure of h2o ice ih. Journal of Physical and Chemical Reference Data, 40(4), 043103.

[16] Zhang, X., Alonso, E.E., Casini, F. (2016). Explicit formulation of at-rest coefficient and its role in calibrating elasto-plastic models for unsaturated soils. Computers and Geotechnics, 71, 56–68.